Journal of Power Sources 191 (2009) 51–57

Contents lists available at ScienceDirect

Journal of Power Sources

journal homepage: www.elsevier.com/locate/jpowsour

# Influence of some metal ions on the structure and properties of doped β-$PbO_2$

N. Chahmana [a], M. Matrakova [b], L. Zerroual [a], D. Pavlov [b,*]

[a] Laboratoire d'Energetique et Electrochimie du Solide (LEES), Universite Ferhat ABBAS, Setif 19000, Algeria
[b] Institute of Electrochemistry and Energy Systems (IEES), BAS, Sofia 1113, Bulgaria

ARTICLE INFO

*Article history:*
Received 2 October 2008
Received in revised form
12 November 2008
Accepted 12 November 2008
Available online 27 November 2008

*Keywords:*
Lead-acid battery
Lead dioxide active mass
Dopant
Lead dioxide structure
Lead dioxide stoichiometry

ABSTRACT

The lead dioxide active mass of positive lead-acid battery plates is a gel-crystal system with proton and electron conductivity of the hydrated gel zones. This paper discusses the influence of $Sn^{2+}$, $Sb^{3+}$, $Co^{2+}$, $Mg^{2+}$ and $Al^{3+}$ ions, added to the formation electrolyte, upon the stoichiometry, structure and phase composition of the $PbO_2$ positive active material (PAM) of lead-acid batteries. PAM samples doped with the above metal ions are characterized by: X-ray diffraction (XRD), thermal gravimetric analysis (TGA), scanning electron microscopy (SEM), inductively coupled plasma atomic emission spectroscopy (ICP-AES) and chemical analysis. The obtained results show that different metal ions are incorporated in different quantities in the $PbO_2$ particles. Under the influence of dopants, the stoichiometric coefficient of lead dioxide decreases, i.e. dopants increase the non-stoichiometry of $PbO_2$. The foreign ions in the formation electrolyte exert strong influence on the microstructure of PAM and change the proportion between crystal and hydrated gel zones in the particles.



## 1. Introduction

The positive lead dioxide active material (PAM) of lead acid batteries is formed by electrochemical oxidation of basic lead sulphates and lead oxide. The capacity of the positive plate depends mainly on the ratio between the two forms of lead dioxide α- and β-$PbO_2$, and on the structure of PAM.

Pavlov [1] has established that the lead dioxide active mass of positive lead-acid battery plates is a gel-crystal system with proton and electron conductivity of the gel (hydrated) zones. Monahov and Pavlov [2] have found hydrated structures in the anodic layer formed on lead electrodes polarized in $H_2SO_4$ solution. At potentials higher than 0.95 V vs. Hg/$Hg_2SO_4$ electrode, $Pb^{4+}$ ions are formed on the electrode surface. These are unstable in water solutions and form $Pb(OH)_4$. The $Pb(OH)_4$ is dehydrated, partially or completely, giving $PbO(OH)_2$ and $PbO_2$. The $PbO_2$ electrode surface is covered by a layer of $PbO(OH)_2$, which layer has gel-like properties. The following equilibrium is established in the electrochemically formed $PbO_2$ particles [1]:

$$\underset{\text{crystal zones}}{PbO_2 + H_2O} \Leftrightarrow \underset{\text{hydrated (gel) zones}}{PbO(OH)_2 \Leftrightarrow H_2PbO_3} \quad (1)$$

The electrochemical reaction of $PbO_2$ reduction during battery discharge proceeds in active centres in the hydrated zones under participation of electrons coming from the crystal zones and protons ($H^+$) coming from the solution (electron–proton mechanism) [1,3,4].

$$PbO(OH)_2 + 2e^- + 2H^+ \rightarrow Pb(OH)_2 + H_2O \quad (2)$$

$$Pb(OH)_2 + H_2SO_4 \rightarrow PbSO_4 + 2H_2O \quad (3)$$

The first stage of PAM discharge is electrochemical and proceeds in the gel zones of particles and agglomerates yielding $Pb(OH)_2$ [4]. Based on the results of kinetic tests and coulometric data Fitas et al. [5] have established that the process of PAM reduction includes two electrochemical stages (one electron is consumed during each stage) taking place in the gel zones according to a proton–electron mechanism or a double-injection process. The role of structural water and $H^+$ ions in the reactivity of the positive active mass has been emphasized by different authors [6–20]. It has been established that heat treatment of PAM results in evaporation of water from the hydrated zones and reduces considerably the proton diffusion coefficient, thus reducing the discharge capacity of the plate. Pavlov and Balkanov have proved experimentally that cations and anions of the solution are involved in ion exchange with $H^+$ and $OH^-$ groups of the gel zones of lead dioxide particles, thus changing the ratio between gel and crystal zones in the particles as well as the composition of the gel zones [20]. This leads to changes in the electrochemical activity of $PbO_2$, which is an open system. Investigations on the maximum admissible levels of various metal ions in electrolyte, PAM, NAM and plate grids of lead-acid batteries, and on their influence on battery performance have been conducted by many authors [21–25]. McGregor provides a classification of additives to the positive active mass that affect $PbO_2$ activity [26].

* Corresponding author. Tel.: +359 29710083; fax: +359 28731552.
*E-mail address:* dpavlov@labatscience.com (D. Pavlov).

0378-7753/$ – see front matter © 2008 Elsevier B.V. All rights reserved.
doi:10.1016/j.jpowsour.2008.11.066

The aim of the present work is to establish the effect of metal ion dopants to the electrolyte for positive plate formation on the structure and degree of hydration of $PbO_2$ particles.

## 2. Experimental

### 2.1. Plate preparation

The paste was prepared from leady oxide (72% PbO) and $H_2SO_4$ solution at 35 °C. The XRD pattern for the starting material evidenced the presence of tetragonal PbO and Pb. Leady oxide (LO) was mixed with water and 1.40 s.g. $H_2SO_4$ in a ratio equal to 5 wt.% $H_2SO_4$/LO. The electroformation process was chosen so that only β-$PbO_2$ was obtained. For the purpose cured plates were soaked in 1.40 s.g. $H_2SO_4$ solution for 18 h and then formed in 1.05 s.g. $H_2SO_4$ solution. Non-doped β-$PbO_2$ was produced by electroformation of cured battery plates in acidic solution. Doped β-$PbO_2$ samples were obtained by adding each dopant to the solution before formation of the plates was completed. Dopants were dissolved in the solution as sulphate salts, antimony was added in the form of $Sb_2O_3$. The initial concentration of each dopant was $10^{-3}$ M and it was selected based on previous works cited in references [22–26]. Analytical grade reagents and distilled water were used for all solutions.

After washing in running water for several hours to remove the excess of sulphuric acid, the plates were dried overnight at 110 °C. Part of the active mass was removed from the grids and ground to powder. This powder was placed in a glass flask and samples of it were then set to X-ray diffraction, thermal and chemical analyses, and SEM examination.

### 2.2. XRD characterization

The positive active materials were characterized by XRD analysis using an APD-15 Philips 2134 diffractometer. The changes in relative intensity of the X-ray characteristic diffraction lines for the different phases in PAM were adopted as a measure of the phase changes in the positive active material under the action of dopants.

### 2.3. Thermal analysis

All tests were performed using an instrument supplied by Mettler Toledo: TGA/SDTA 851e. All measurements were carried out in Nitrogen atmosphere at a gas flow-rate of 50 $cm^3\,min^{-1}$ and at a constant heating rate of 2 $K\,min^{-1}$. All samples were dried at 60 °C to evaporate the surface adsorbed water.

## 3. Results and discussion

### 3.1. Chemical analysis of PAM with dopants

Table 1 summarizes the obtained results for the chemical composition of PAM formed in solutions with different dopants. The different metal ions are incorporated in the $PbO_2$ particles in different amounts thus reducing the quantity of $Pb^{4+}$ ions. It is well known that lead dioxide is non-stoichiometric. Under the action of dopants its stoichiometric coefficient decreases from 1.966 to an average of 1.915, i.e. dopants increase the non-stoichiometry of $PbO_{2-x}$ by 2.6%. Data in the third column of Table 1 indicate that $Sn^{2+}$ ions reduce most pronouncedly the stoichiometric coefficient $(2-x)$ from 1.966 to 1.908, i.e. by 3%. Next in power of influence are $Sb^{3+}$ ions, which decrease the stoichiometric coefficient down to 1.912.

**Table 1**
Results from chemical analysis and ICP-AES analysis of PAM formed in solutions with dopants.

| Sample name | $PbO_2$ | PbO | $PbO_{(2-x)}$ | $PbSO_4$ | % dopant (ICP-AES) |
|---|---|---|---|---|---|
| β-$PbO_2$-E | 93.59 | 3.26 | 1.966 | 1.93 | |
| β-$PbO_2$ + $Mg^{2+}$ | 87.57 | 7.31 | 1.922 | 3.25 | 0.0006 |
| β-$PbO_2$ + $Al^{3+}$ | 90.12 | 8.03 | 1.918 | – | <0.0002 |
| β-$PbO_2$ + $Co^{2+}$ | 90.09 | 8.10 | 1.917 | – | 0.1 |
| β-$PbO_2$ + $Sn^{2+}$ | 85.29 | 8.65 | 1.908 | 2.79 | 0.1 |
| β-$PbO_2$ + $Sb^{3+}$ | 87.72 | 8.48 | 1.912 | 1.73 | 0.02 |

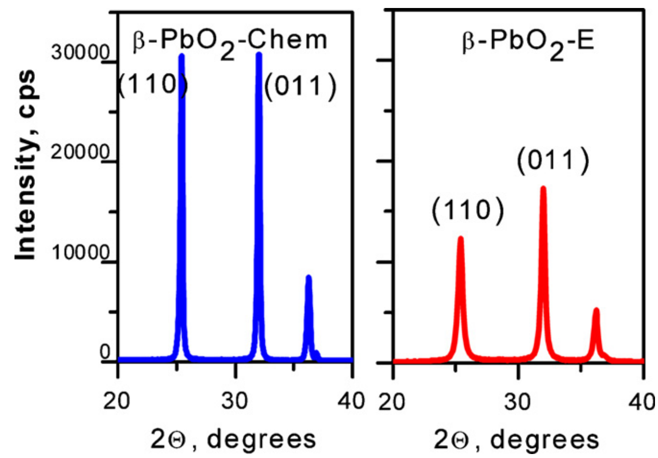


**Fig. 1.** XRD patterns for a chemical product β-$PbO_2$-Chem and for an electrochemically obtained β-$PbO_2$-E.

### 3.2. XRD analysis of PAM with dopants

The XRD data indicate that all PAM samples comprise mostly β-$PbO_2$ crystal phase. Fig. 1 shows XRD patterns for chemically and electrochemically (PAM-E) obtained lead dioxide. For PAM-E (non-doped) the characteristic diffraction line (0 1 1) has the highest intensity, whereas for the chemically obtained β-$PbO_2$ sample both diffraction lines (1 1 0) and (0 1 1) have equal intensity, and it is twice higher than that of the (0 1 1) diffraction line for PAM-E.

Fig. 2 presents XRD patterns for PAM doped with $Mg^{2+}$, $Sb^{3+}$ or $Al^{3+}$. The diffractograms for the samples doped with $Mg^{2+}$ or $Sb^{3+}$ evidence the presence of a $PbSO_4$ phase, while the PAM sample doped with $Al^{3+}$ contains also α-$PbO_2$.

The peak intensity of diffraction line (1 1 0) for β-$PbO_2$ and the crystal size values for samples with different dopants are presented in Fig. 3. The crystal size has been calculated from the full width at half maximum (FWHM) of the (1 1 0) diffraction line for β-$PbO_2$ using Sherrer equation.

The data in Fig. 3 indicate that the chemically obtained product β-$PbO_2$ has the highest crystallinity and the largest crystals. The electrochemically obtained β-$PbO_2$-E yields diffraction lines of half the intensity of the chemically obtained product and smaller crystallite sizes. $Sn^{2+}$ and $Sb^{3+}$ ions cause the most pronounced reduction in β-$PbO_2$ crystal size. The XRD pattern for the sample doped with $Sn^{2+}$ features the lowest intensity of the diffraction lines and the smallest crystallite size values. This sample yields also a broader (0 1 1) peak, which according to [16], is also indicative of smaller crystallites. Such diffractograms may be attributed to amorphous phases and to $H_2O$ incorporated into the β-$PbO_2$ structure [17]. $Co^{2+}$ ions added to the solution lead to formation of larger β-$PbO_2$ crystals than those formed in non-doped electrolyte. $Mg^{2+}$ and $Al^{3+}$ ions exert but a slight influence on the size of β-$PbO_2$ particles formed in PAM.

It was found from the XRD patterns that the peaks for the samples containing $Sn^{2+}$, $Sb^{3+}$, $Mg^{2+}$ or $Al^{3+}$ shift slightly to higher diffraction angle than that for non-doped PAM. In contrast, the sam-

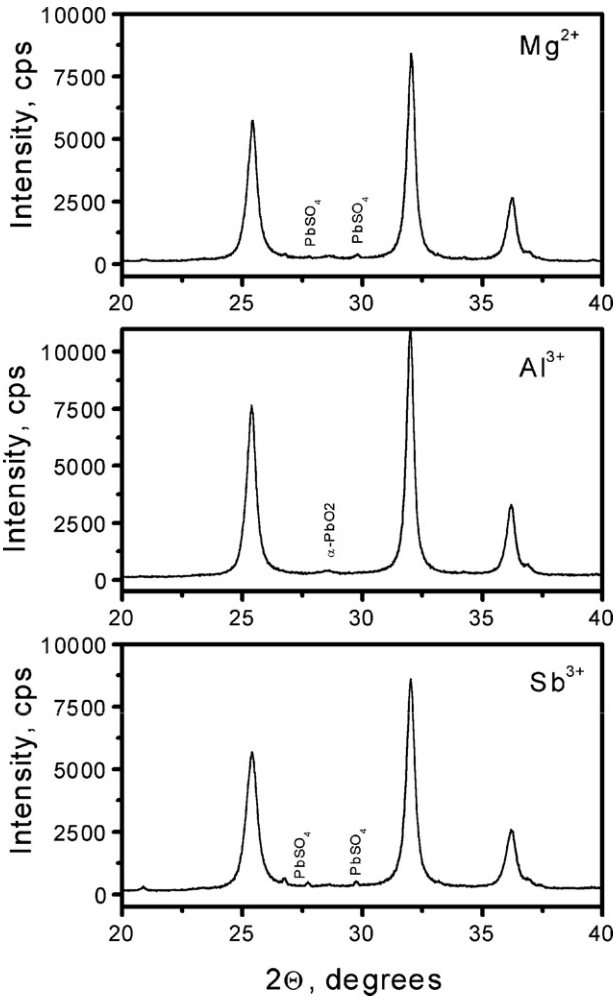


**Fig. 2.** XRD patterns for PAM doped with $Mg^{2+}$, $Al^{3+}$ or $Sb^{3+}$.

ple doped with $Co^{2+}$ features XRD peaks shifted to lower diffraction angle. This indicates that the interplanar distance has changed, which implies that the different cations have been incorporated into the β-$PbO_2$ crystal lattice.

*3.3. SEM examination of the microstructure of PAM with dopants*

Fig. 4 presents SEM pictures of $PbO_2$ particles and aggregates of PAM formed in electrolytes containing different dopant ions, and in non-doped solutions.

When formed in solution with no additives, the PAM comprises $PbO_2$ particles grouped in small agglomerates, which coalesce into an aggregate. $Al^{3+}$ or $Sb^{3+}$ ions added to the formation electrolyte facilitate closer interconnection of $PbO_2$ particles in agglomerates but individual nanoparticles are still distinguished. The ability of $Sb^{3+}$ ions to stimulate coalescence of $PbO_2$ particles into aggregates has been observed also by Giess [27]. Other ions, $Co^{2+}$, $Mg^{2+}$ and $Sn^{2+}$, facilitate the formation of bigger, clearly pronounced individual $PbO_2$ particles.

Based on the obtained SEM data it can be generally concluded that foreign ions in the formation electrolyte exert strong influence on the microstructure of PAM.

*3.4. Thermogravimetric analysis of PAM with different dopants*

The thermal analyses were performed within the temperature range from 25 to 370 °C, as the aim of these analyses was to determine the hydrated parts of the samples. Fig. 5 presents the measured weight losses for PAM samples with different dopants as a function of heating temperature. Table 2 gives total weight loss data for the investigated samples. All dopants, except $Mg^{2+}$, facilitate the hydration of PAM. A more than double increase in weight loss is observed with the sample doped with $Sn^{2+}$ as compared to all other samples.

Four temperature zones of weight loss can be distinguished. *A-zone*: from 25 to 75 °C, in this temperature interval the measured weight losses are due to evaporation of weakly bound (surface adsorbed) water. *B-zone*: from 75 to 215 °C, in this temperature interval weight losses are related to the release of $H_2O$ from the hydrated (gel) part of PAM particles and agglomerates. *C-zone*: from 215 to 325 °C, weight losses at these temperatures are due to evaporation of the water that is strongly bound to the lead dioxide particles. *D-zone*: at temperatures higher than 325 °C decomposition of β-$PbO_2$ and formation of non-stoichiometric $PbO_n$ $(1 < n < 2)$ starts [10].

In addition to the obtained TGA curves, derivative thermogravimetric curves (DTG: 1st derivative of TGA curve) were also plotted to aid interpretation of the results. A DTG curve gives the

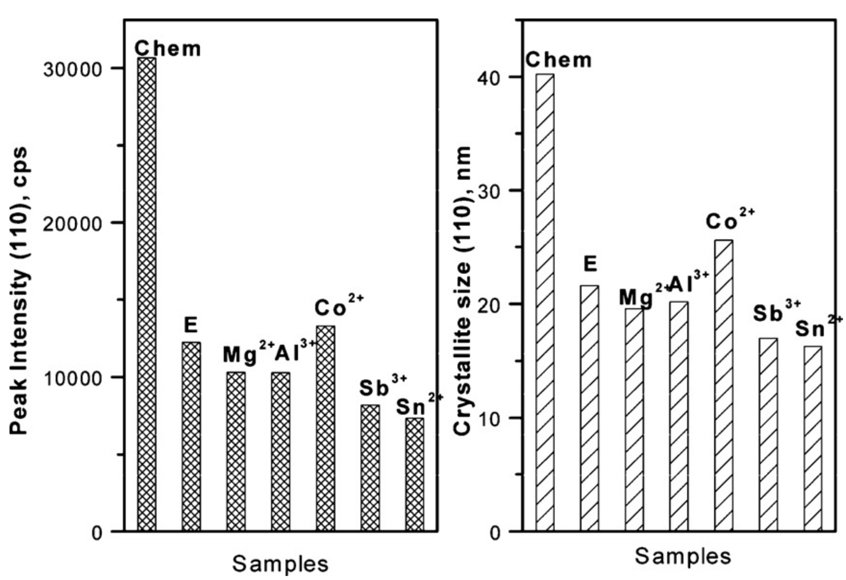


**Fig. 3.** Peak intensity of the β-$PbO_2$ diffraction line (1 1 0) and crystallite size for PAM samples with different dopants.

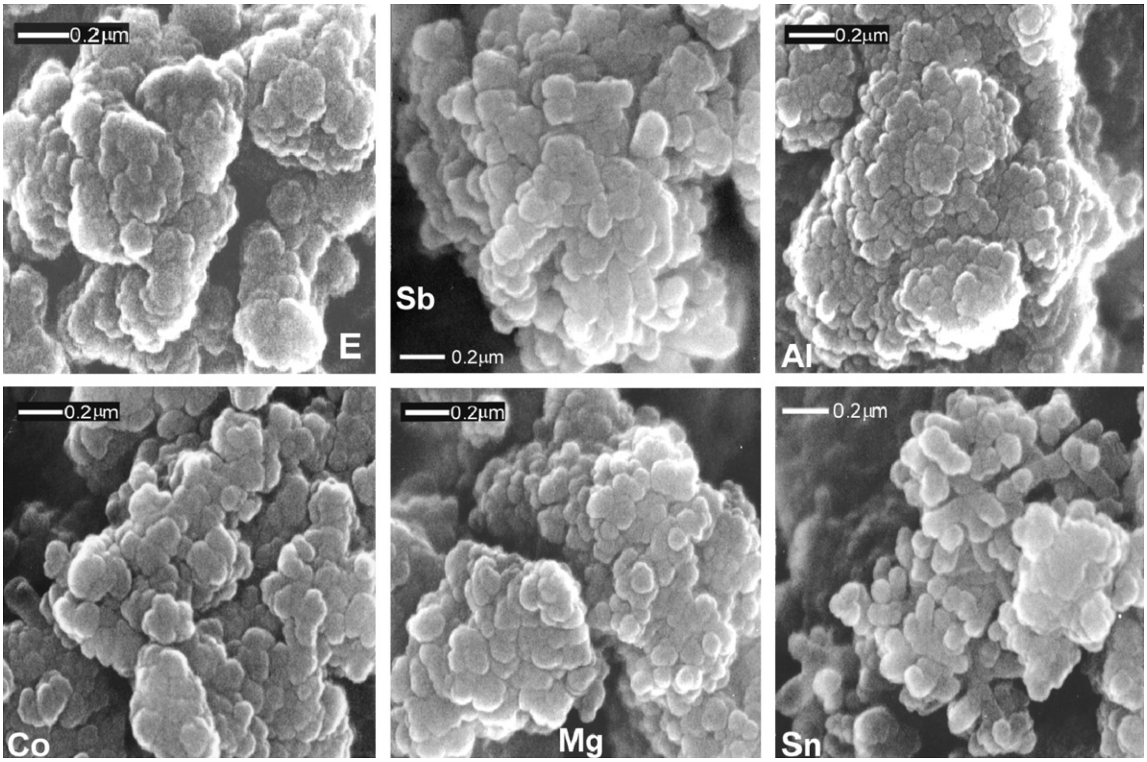


**Fig. 4.** SEM images of PAM samples formed in solution with no additives and with addition of dopants.

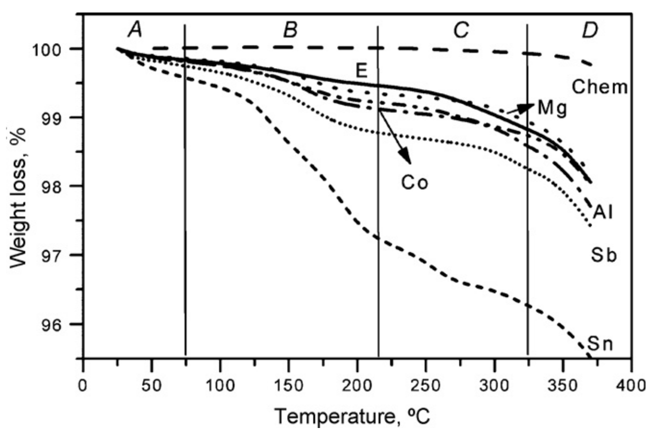


**Fig. 5.** TGA curves for PAM formed in solutions with dopants and in non-doped solution.

weight loss on temperature increase by 1 °C. Fig. 6 presents the obtained DTG curves for the investigated samples.

It is evident from the data in the figure that water in the gel zones of PAM doped with $Sn^{2+}$ ions is bound in four different ways and evaporates in four temperature steps: at 134, 147, 188 and 253 °C, thus yielding four peaks in the DTG curves. The data in Table 1 indicate that the $PbO_2$ particles of PAM doped with 0.1% $Sn^{2+}$ have the lowest stoichiometric coefficient compared to the other PAM samples. Second in terms of quantity of hydration water (chemisorbed water) contained is the PAM sample with $Sb^{3+}$. The greatest quantity of water evaporates at 166 °C. The different profiles of the DTG curves for PAM($Sn^{2+}$) and PAM($Sb^{3+}$) indicate that, depending on the dopant used, the water in the gel zones is bound in different manner. Non-doped PAM and PAM doped with $Mg^{2+}$, $Al^{3+}$ or $Co^{2+}$ produce one DTG temperature peak at about 160 °C, i.e. within the *B* temperature zone. In the *C-zone*, at temperatures above 300 °C, the measured weight losses of these samples can be attributed to either water evaporation or to evolution of oxygen from the $PbO_2$ structure.

Fig. 7 presents the weight losses of the investigated samples in the temperature zones *A*, B and C, as well as the overall weight loss of the respective samples.

**Table 2**
Results from TGA analysis of PAM formed in solutions with dopants and in un-doped solution.

| Sample | Total weight loss (%) |
|---|---|
| β-$PbO_2$-Chem | 0.2670 |
| β-$PbO_2$-E | 1.9325 |
| $Mg^{2+}$ | 1.8166 |
| $Al^{3+}$ | 2.2797 |
| $Co^{2+}$ | 1.9708 |
| $Sn^{2+}$ | 4.4701 |
| $Sb^{3+}$ | 2.5616 |

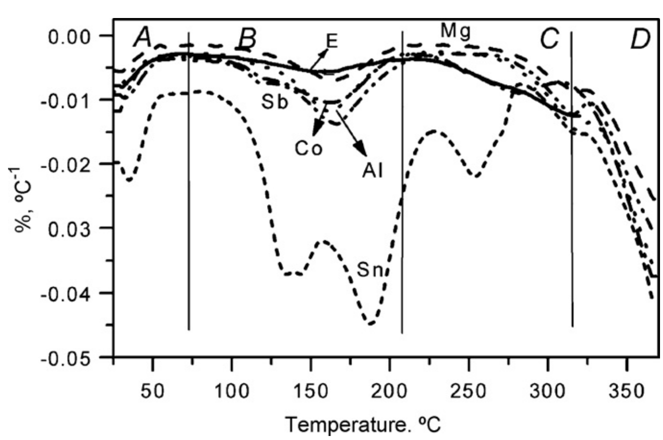


**Fig. 6.** DTG curves for PAM formed in solutions with dopants and in non-doped solution.

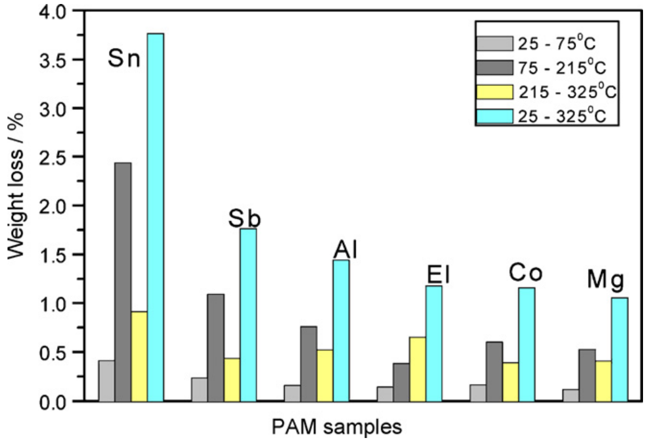


**Fig. 7.** Weight loss data (%) for doped and non-doped PAM samples on heating at different temperatures.

The obtained weight loss data and the XRD data about the crystallite sizes of the various PAM samples (Fig. 3), give grounds for the following general conclusion: the higher the crystallinity of PAM the lower the hydration of the lead dioxide particles. This finding indicates that PAM particles represent a dynamic system in which the following processes take place:

$$\underset{\text{crystal zones}}{PbO_2 + H_2O} \Leftrightarrow \underset{\text{hydrated (gel) zones}}{PbO(OH)_2 \Leftrightarrow H_2PbO_3} \quad (1)$$

When dopant ions ($Me^{2+}$) from the solution are exchanged with $H^+$ ions from $H_2PbO_3$ "$MePbO_3$" is formed:

$$H_2PbO_3 + Me^{2+} \Leftrightarrow MePbO_3 + 2H^+ \quad (4)$$

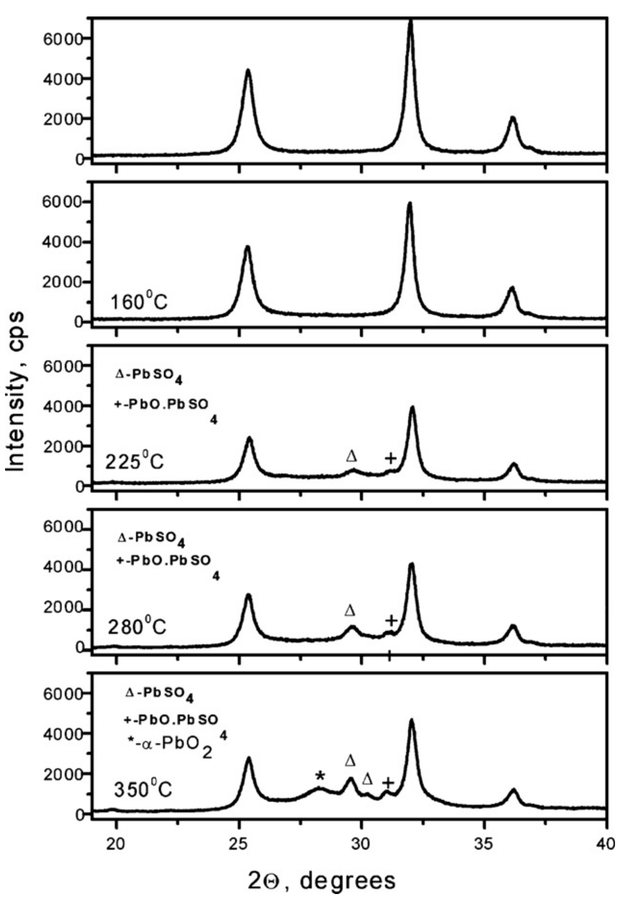


**Fig. 8.** XRD patterns for PAM ($Sn^{2+}$) heated to different end temperatures.

Incorporation of $Me^{2+}$ ions into the gel zones of $PbO_2$ particles does not lead to formation of new compounds, but rather to inclusion of the $Me^{2+}$ ions into the structure of $PbO(OH)_2$ or $H_2PbO_3$. In order to sustain equilibrium (1), new water quantities enter the gel zones and consequently $PbO(OH)_2$ is formed. The crystallinity of the particles decreases while the share of the gel zones increases. On comparing the amounts of water entering the investigated samples (Fig. 7) and the changes in crystallinity of the respective PAM this water causes (Fig. 3), it becomes evident that they are not strictly equivalent. This means that dopants change not only the quantity of the hydrated part (i.e. $PbO(OH)_2$) of PAM particles, but also the ratio between the crystal and amorphous parts of solid state lead dioxide. The minimums in the DTG curves (Fig. 6) signify different

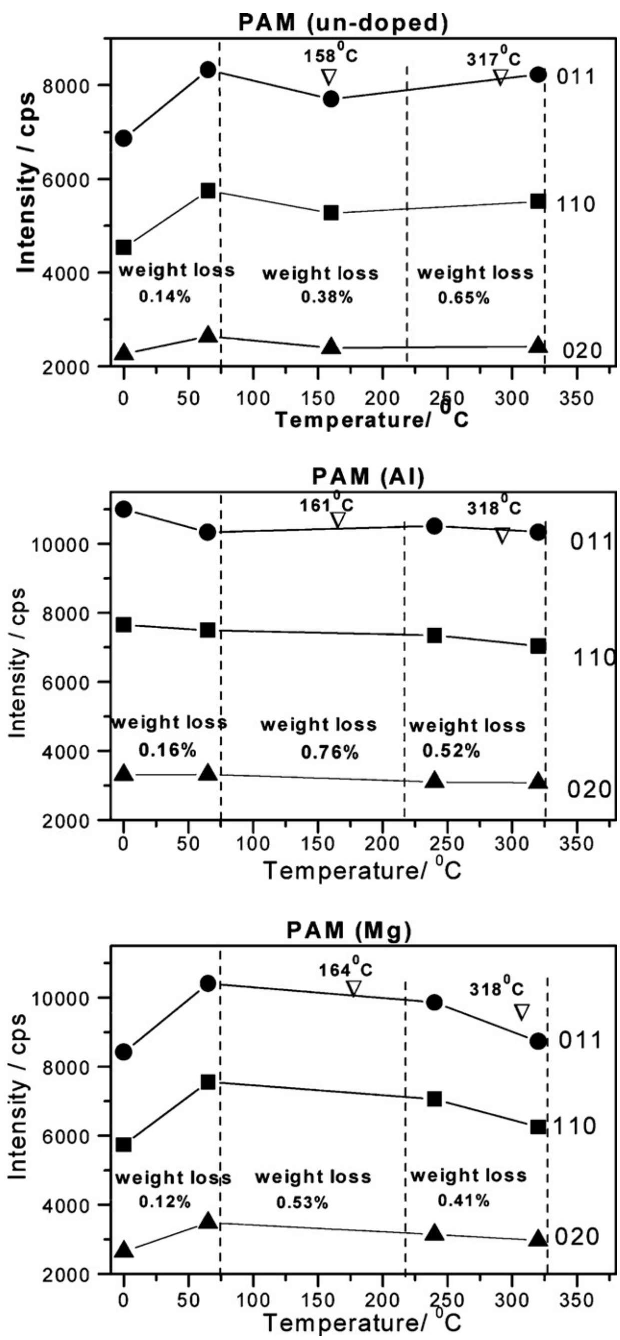


**Fig. 9.** Changes in intensity of the XRD peaks for β-$PbO_2$ on heating electrochemically obtained (non-doped) PAM(E), PAM($Al^{3+}$) and PAM($Mg^{2+}$) samples to different temperatures.

bonds of $H_2O$ and dopant ions in the gel zones structure. This is most evident in the DTG curves for PAM($Sn^{2+}$) and PAM($Sb^{3+}$).

Fig. 8 presents the XRD patterns for PAM($Sn^{2+}$) heated to different end temperatures. When the samples are heated to end temperature between 160 and 225 °C, two new crystal phases are formed: $PbSO_4$ and PbO.$PbSO_4$. As evident from the data in Table 1, PAM($Sn^{2+}$) has the lowest stoichiometric coefficient: $PbO_{1.908}$. There is a significant quantity of $Pb^{2+}$ and $Pb^{3+}$ ions incorporated in the crystal lattice of $PbO_2$ or in the gel zones, which reduce its stoichiometric coefficient. The hydrated zones in β-$PbO_2$ particles contain some $Pb^{2+}$ and $SO_4{}^{2-}$ ions. On heating of the samples water evaporates, $Pb^{2+}$ and $SO_4{}^{2-}$ ions regroup, and $PbSO_4$ and PbO.$PbSO_4$ crystals are formed. At temperatures higher than 325 °C, decomposition of β-$PbO_2$ and formation of α-$PbO_2$ starts.

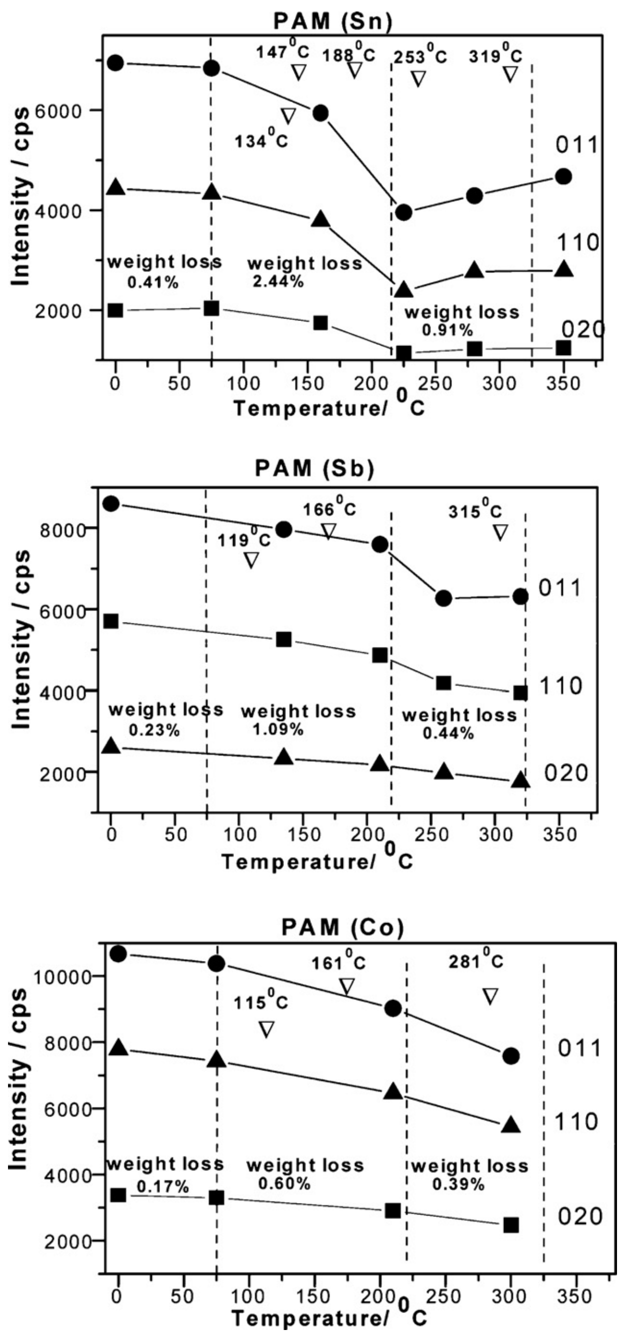


**Fig. 10.** Changes in intensity of the XRD peaks for β-$PbO_2$ on heating PAM($Sn^{2+}$), PAM($Sb^{3+}$) and PAM($Co^{2+}$) samples to different temperatures.

These processes are observed only in PAM($Sn^{2+}$), which indicates that $Sn^{2+}$ ions affect both the structure and stoichiometry of $PbO_2$. This effect holds for the crystalline and amorphous parts of $PbO_2$ particles.

Upon heating PAM samples with various dopants structural changes occur in both the crystalline and the hydrated parts of PAM. These changes can be followed by a combination of XRD and DTG analyses. Fig. 9 presents the changes in intensity of the XRD peaks for β-$PbO_2$ on heating electrochemically obtained (non-doped) PAM(E), PAM($Al^{3+}$) and PAM($Mg^{2+}$) samples to different temperatures. The weight losses at the three temperature steps of dehydration as well as the respective DTG peak temperatures are also presented in the figure.

When heated to 75 °C, non-doped PAM(E) and PAM($Mg^{2+}$) increase their crystallinity, which indicates that part of the water is weakly bound to β-$PbO_2$.

On further temperature increase up to 325 °C, PAM(E) and PAM($Al^{3+}$) are dehydrated (lose weight), but no change in crystallinity of $PbO_2$ is observed. In contrast, the curve for PAM($Mg^{2+}$) evidences a decrease in relative intensity of the XRD peak for β-$PbO_2$, which is an indication of amorphization of the lead dioxide as a result of dehydration.

The changes in intensity of the β-$PbO_2$ diffraction peaks on heating PAM($Sn^{2+}$), PAM($Sb^{3+}$) and PAM($Co^{2+}$) to different temperatures are presented in Fig. 10.

Five DTG peaks are observed for PAM($Sn^{2+}$), against three for PAM($Sb^{3+}$) and PAM($Co^{2+}$) samples. Heating of PAM($Sb^{3+}$) to 210 °C leads to amorphization of β-$PbO_2$. In the case of PAM($Sb^{3+}$) and PAM($Co^{2+}$) samples, amorphization due to dehydration continues on further heating to higher temperatures, too. Heating PAM($Sn^{2+}$) in the range from 225 to 350 °C results in partial crystallization of the amorphous β-$PbO_2$. Each dopant, even in small quantities, exerts its specific influence upon the structure of the crystal and hydrated parts of PAM.

The results of the present investigation demonstrate that even small quantities of dopants exert strong influence upon the structure of PAM and it can be expected that they will also affect its electrochemical activity.

## 4. Conclusions

Electrochemically obtained $PbO_2$ comprises particles and agglomerates with crystal and hydrated (gel) zones, which are in equilibrium with ions of the solution. This $PbO_2$ is electrochemically active and is used as positive electrode in lead acid batteries. The present work investigates the influence of $Sn^{2+}$, $Sb^{3+}$, $Co^{2+}$, $Mg^{2+}$ and $Al^{3+}$ ions added to the formation electrolyte upon the stoichiometry, structure and phase composition of the $PbO_2$ positive active material in lead-acid batteries. It has been established that small quantities of the above listed ions (dopants) incorporate into PAM and reduce the stoichiometric coefficient of the electrochemically obtained $PbO_{2-x}$. Except for $Co^{2+}$, metal ions increase the share of hydrated (gel) zones in PAM. Dopants affect the interconnection of $PbO_2$ particles into agglomerates by intensifying ($Co^{2+}$, $Sn^{2+}$, $Mg^{2+}$) or reducing ($Sb^{3+}$ and $Al^{3+}$) their individuality when forming agglomerates and aggregates in the structure of PAM.

The influence of dopants on the electrochemical characteristics of the $PbO_2$/$PbSO_4$ electrode will be the subject of a separate paper to follow.

## References


[1] D. Pavlov, J. Electrochem. Soc. 139 (1992) 3075.
[2] B. Monahov, D. Pavlov, J. Appl. Electrochem. 23 (1993) 1244.
[3] D. Pavlov, I. Balkanov, P. Rachev, J. Electrochem. Soc. 134 (1992) 2390.
[4] D. Pavlov, I. Balkanov, T. Halachev, P. Rachev, J. Electrochem. Soc. 136 (1989) 3189.

[5] R. Fitas, N. Chelali, L. Zerroual, B. Djellouli, Solid State Ionics 127 (2000) 49.
[6] A.C. Simon, S.M. Caulder, J.T. Stemmle, J. Electrochem. Soc. 122 (1975) 461.
[7] P.T. Moseley, J.L. Hutchinson, C.J. Wright, M.A. Bourke, R.J. Hill, V.S. Rainey, J. Electrochem. Soc. 130 (1983) 829.
[8] R.J. Hill, A.M. Jessel, J. Electrochem. Soc. 134 (1987) 1326.
[9] J. Yamashita, Y. Matsumaru, J. Appl. Electrochem. 18 (1988) 595.
[10] D. Pavlov, E. Bashtavelova, V. Manev, A. Nasalevska, J. Power Sources 19 (1987) 15.
[11] R.J. Hill, M.R. Houchin, Electrochim. Acta 30 (1985) 559.
[12] I. Peterson, E. Ahlberg, J. Power Sources 91 (2000) 137.
[13] D. Pavlov, A. Kirchev, M. Stoycheva, B. Monahov, J. Power Sources 137 (2004) 288.
[14] R. Fitas, L. Zerroual, N. Chelali, B. Djellouli, J. Power Sources 64 (1997) 57.
[15] J. Morales, G. Petkova, M. Cruz, A. Caballero, J. Power Sources 158 (2006) 831.
[16] L. Zerroual, R. Fitas, B. Djellouli, N. Chelali, J. Power Sources 158 (2006) 837.
[17] U. Hullmeine, A. Winsel, E. Voss, J. Power Sources 25 (1989) 27.
[18] E. Meissner, E. Voss, J. Power Sources 33 (1991) 231.
[19] R. Fitas, L. Zerroual, N. Chelali, B. Djellouli, J. Power Sources 58 (1996) 225.
[20] D. Pavlov, I. Balkanov, J. Appl. Electrochem. 139 (1992) 1830.
[21] J.R. Pierson, C.E. Weinlein, C.E. Wright, in: D.H. Collins (Ed.), Power Sources 5. Research and Development in Non-Mechanical Electrical Power Sources, Academic Press, New York, 1975, p. 97.
[22] B.K. Mahato, W.H. Tiedemann, J. Electrochem. Soc. 130 (1983) 2139.
[23] L.T. Lam, J.D. Douglas, R. Pillig, D.A.J. Rand, J. Power Sources 48 (1994), 219–232 219.
[24] H. Sanchez, Y. Meas, I. Gonzalez, M.A. Quiroz, J. Power Sources 32 (1990) 43–5343.
[25] M. Maja, N. Penzzi, J. Power Sources 22 (1988) 1–9.
[26] K. McGregor, J. Power Sources 59 (1996) 31.
[27] H. Giess, private communication.